



Global warming increases the frequency of river floods in Europe

L. Alfieri, P. Burek, L. Feyen, and G. Forzieri

European Commission – Joint Research Centre, Ispra, Italy

Correspondence to: L. Alfieri (lorenzo.alfieri@jrc.ec.europa.eu)

Received: 19 December 2014 – Published in Hydrol. Earth Syst. Sci. Discuss.: 23 January 2015

Accepted: 25 April 2015 – Published: 11 May 2015

Abstract. EURO-CORDEX (Coordinated Downscaling Experiment over Europe), a new generation of downscaled climate projections, has become available for climate change impact studies in Europe. New opportunities arise in the investigation of potential effects of a warmer world on meteorological and hydrological extremes at regional scales. In this work, an ensemble of EURO-CORDEX RCP8.5 scenarios is used to drive a distributed hydrological model and assess the projected changes in flood hazard in Europe through the current century. Changes in magnitude and frequency of extreme streamflow events are investigated by statistical distribution fitting and peak over threshold analysis. A consistent method is proposed to evaluate the agreement of ensemble projections. Results indicate that the change in frequency of discharge extremes is likely to have a larger impact on the overall flood hazard as compared to the change in their magnitude. On average, in Europe, flood peaks with return periods above 100 years are projected to double in frequency within 3 decades.

terns are still under investigation, especially when extreme events are considered (Andersen and Marshall Shepherd, 2013). Climate projections are produced by global circulation models (GCMs) or earth system models (ESMs) and are then downscaled on smaller domains using regional climate models (RCMs) to provide higher-resolution information for regional simulations. Assessments of the future flood hazard over large domains are commonly performed by coupling atmospheric climate projections with land-surface schemes and hydrological models (e.g. Alkama et al., 2013; Arnell and Gosling, 2014; Dankers et al., 2013; Sperna Weiland et al., 2012). At the European scale, high-resolution future flood hazard projections currently available are mostly based on the Special Report on Emissions Scenarios (SRES) produced for the Third and Fourth Assessment Reports (McCarthy, 2001; IPCC, 2007) of the Intergovernmental Panel on Climate Change (IPCC). Relevant examples are the works by Dankers and Feyen (2008, 2009) and more recently by Rojas et al. (2012), who used downscaled climate scenarios for Europe produced in the context of the PRUDENCE (Christensen et al., 2007) and ENSEMBLES (Van der Linden and Mitchell, 2009) projects. The Coordinated Downscaling Experiment over Europe (EURO-CORDEX; Jacob et al., 2014) represents the new generation of high-resolution climate projections up to 2100, based on the fifth phase of the Coupled Model Intercomparison Project (CMIP5; Taylor et al., 2012). EURO-CORDEX includes an ensemble of consistent scenarios based on the latest model versions available and offers the opportunity to update and possibly improve current estimates of future flood hazard in Europe.

In this work, ensemble streamflow simulations from 1976 to 2100 are produced using seven EURO-CORDEX climate projections fed into a distributed hydrological model. The chosen climate projections are forced by Representative Concentration Pathway (RCP) 8.5 W m^{-2} , to simulate the ef-

1 Introduction

Every year, new record-breaking hydrological extremes affect our society, fuelling the debate between climate change and natural climate variability. The increasing availability of long time series of hydro-meteorological observations enabled the identification of unequivocal and statistically significant anthropogenic changes of atmospheric and climatic variables such as CO_2 concentration and air temperature (IPCC, 2013). The Clausius–Clapeyron equation indicates that warmer air temperature is linked to increasing atmospheric water vapour content, which in turn determines the total precipitable water. Yet, regional implications of ongoing global warming on future precipitation and runoff pat-

fect on the projected river streamflow of high-end emission scenarios corresponding to the exceedance of 4 °C globally by the end of the current century (IPCC, 2013). Projected changes in the magnitude and frequency of different hydro-meteorological variables are investigated to assess future changes in flood hazard in Europe. Differently to previous works, raw model output is used rather than bias-corrected scenarios. A number of scientific works support the idea that errors in the shape of the temperature and precipitation pdfs (probability density functions) are corrected adequately by bias correction techniques in a range of values around the mean but do not improve the representation of extremes (Ehret et al., 2012; Huang et al., 2014; Muerth et al., 2013; Themeßl et al., 2012). Furthermore, a number of processed data sets are produced at a spatial resolution coarser than the original one, to conform to the available gridded observations, thus limiting the range of applications at the small scale. The idea pursued in this work is to make use of the original resolution of climate scenarios, particularly important to simulate the dynamics of streamflow extremes, and express the results of future projections as relative changes from baseline scenarios rather than absolute values. Statistical robustness is sought through the use of ensemble projections and through data aggregation over time (i.e. 30-year time slices) and space (i.e. country and river basin level) with the goal of detecting statistically significant trends over time and with regard to extreme events.

2 Data

The work presented focuses on the European region, where boundaries follow the hydrographic divides as shown in Fig. 1 (dark grey). The statistical analyses are based on the hydrological model output, which is set up at a 5 km × 5 km spatial resolution and daily time step. The following two sections describe some details of the meteorological variables extracted from the climate projections and of the hydrological model used to estimate streamflow data over the simulation domain.

2.1 Climate projections

EURO-CORDEX historical climate scenarios and future projections with RCP8.5 were used in this study to produce river streamflow simulations in Europe over the period 1970–2100 under a high-end global warming scenario. These projections consist of high-resolution downscaling of GCMs from the CMIP5 and can be downloaded from different data nodes of the Earth System Grid Federation (e.g. <http://esgf-data.dkrz.de>) or from the Climate4Impact portal (<http://climate4impact.eu>). The seven models were chosen among those available in mid 2014, giving priority to models with driving GCMs with high ranking in the performance evaluation of CMIP5 models carried out by Perez et al. (2014).

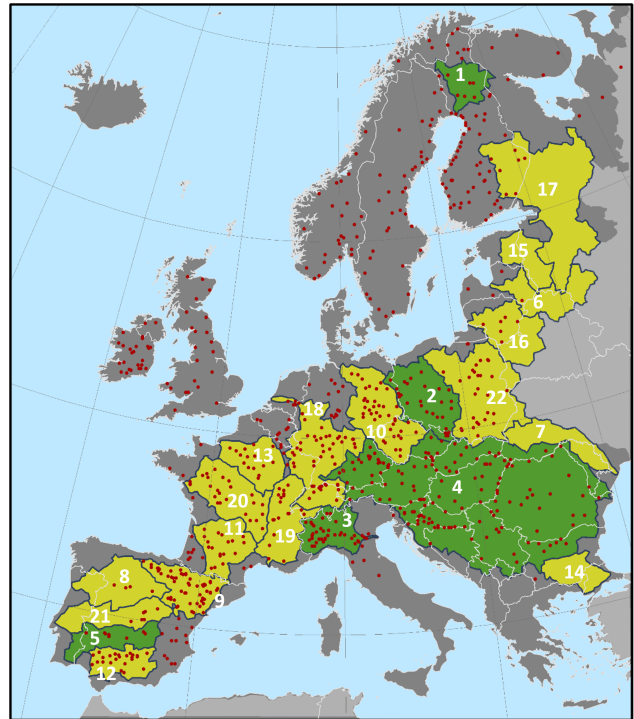


Figure 1. Map of the simulation domain with selected river basins analysed in the text (in green) and in the Supplement (in yellow). Discharge stations where the Lisflood model was calibrated are shown with red points.

Daily historical simulations from 1970 to 2005 and climate projections with RCP8.5 from 2006 to 2100 at 0.11° horizontal resolution (~ 12 km) were extracted for seven EURO-CORDEX scenarios. Overall, the seven climate scenarios are combinations of three different GCMs which were then downscaled with four RCMs as shown in Table 1. Meteorological fields used in this work are average (tas), minimum (tasmin) and maximum (tasmax) surface air temperature, total precipitation (pr), surface air pressure (ps), 2 m specific humidity (huss), 10 m wind speed (sfcWind) and surface downwelling shortwave radiation (rsds).

2.2 Hydrological model

The Lisflood model is used in this work to perform hydrological simulations using gridded meteorological variables extracted from the climate scenarios. Lisflood (Burek et al., 2013b; van der Knijff et al., 2010) is a distributed semi-physically based rainfall–runoff model combined with a routing module for river channels. Processes simulated include canopy and surface processes, snow accumulation and melting, soil and groundwater processes, streamflow and water abstraction in the river network. Lisflood was originally designed for large river basins (De Roo et al., 2001; Thiemeig et al., 2013), though it has shown skilful performance in applications to a wide range of basin sizes (e.g. Alfieri et al., 2012;

Table 1. EURO-CORDEX climate scenarios used in this study.

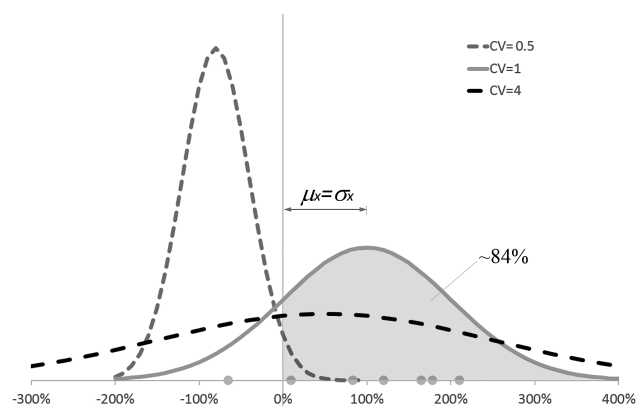
	Institute	GCM	RCM	Driving ens. member	Res. [°]	RCP	Calendar
1	KNMI	EC-EARTH	RACMO22E	r111p1	0.11	8.5	Standard
2	SMHI	HadGEM2-ES	RCA4	r111p1	0.11	8.5	360 day
3	SMHI	EC-EARTH	RCA4	r1211p1	0.11	8.5	Standard
4	MPI-CSC	MPI-ESM-LR	REMO2009	r111p1	0.11	8.5	Proleptic Gregorian
5	CLMcom	MPI-ESM-LR	CCLM4-8-17	r111p1	0.11	8.5	Proleptic Gregorian
6	SMHI	MPI-ESM-LR	RCA4	r111p1	0.11	8.5	Proleptic Gregorian
7	CLMcom	EC-EARTH	CCLM4-8-17	r1211p1	0.11	8.5	Proleptic Gregorian

Thirel et al., 2012; Wanders et al., 2014; Younis et al., 2008). Lisflood is the operational model adopted by the European Flood Awareness System (Thielen et al., 2009) and thanks to this the European setup is subject to periodical parameter calibration exercises, to include new discharge observations and update existing time series with recent data. In the current model setup, Lisflood is calibrated with the standard particle swarm 2011 algorithm (Zambrano-Bigiarini and Rojas, 2014) at 693 stations across Europe (see Fig. 1). The model calibration is based on up to 8 years of daily data using the EFAS-Meteo data set (Ntegeka et al., 2013) as meteorological input data and a network of observed discharge time series at the calibrated stations. The latest developments on the European setup include the simulation of 182 lakes and 34 large reservoirs, and the implementation of monthly maps of water use from the SCENES project (Kamari et al., 2008), which for this work are assumed constant throughout the current century.

3 Methods

Statistical and quantitative analyses shown in this article compare a historical (i.e. present day) scenario with three future time slices, all four of 30-year durations. The historical scenario is assumed over the period 1976–2005, leaving out the first 6 years of the data set as warm-up period for the hydrological simulations and thus achieve a better representation of the model’s initial conditions; hereinafter referred to as “baseline” or “1990”, after the median year of the time slice. Similarly, future time slices span over the windows 2006–2035, 2036–2065, 2066–2095, and are referred to as “2020”, “2050”, and “2080”, respectively.

Most quantitative analyses shown in the remainder are targeted to assessing the relative changes Δx of a projected variable (x_f) for a future time slice towards the corresponding baseline value (x_b). The consistency of the $i = \{1, \dots, N\}$ model projections is evaluated through the use of the coefficient of variation (CV) of the relative change,

**Figure 2.** Schematic view of the coefficient of variation of the relative error.

$$CV_{\Delta x} = \frac{\sigma_{\Delta x}}{|\mu_{\Delta x}|} = \frac{\sqrt{\sum \forall i (\Delta x_i - \bar{\Delta x})^2}}{|\bar{\Delta x}|}, \quad (1)$$

which is calculated as the ratio between the standard deviation of the ensemble of relative changes $\sigma_{\Delta x}$ and their mean absolute values of the baseline $|\mu_{\Delta x}|$. Smaller CVs indicate models agreement on the projected mean change, where the ensemble members are spread over a relatively narrow window compared to the magnitude of the change. Larger CVs suggest a more uncertain trend, with values scattered between positive and negative changes (see Fig. 2). To reduce the misinterpretation of results a stringent value of $CV = 1$ is chosen as threshold, so that larger values are greyed out in the figures of projected changes. If one assumes that relative changes are normally distributed, the condition $CV = 1$ corresponds to an 84 % probability of changes having the same sign (i.e. positive or negative), which for this example roughly corresponds to an average agreement of six out of seven models (i.e. 86 %). Furthermore, for comparison with the IPCC terminology for likelihood (e.g. Field et al., 2014, p. 41), it fits between the classes likely ($> 66\%$) and very likely ($> 90\%$).

3.1 Trend analysis of precipitation

The first part of the study focuses on the analysis of precipitation patterns of the seven climate scenarios. Considered variables are annual precipitation (pr_{Year}) and annual maximum daily precipitation (pr_{MAX}). The average change between the three future time slices and the baseline is evaluated on a spatial basis, by assessing the agreement of the ensemble projections with the above described coefficient of variation of the relative change.

In a subsequent step, the two precipitation-related variables are aggregated over 22 European river basins with upstream area at the outlet larger than 50 000 km². The trend of annual values of basin-aggregated pr_{Year} and pr_{MAX} is then investigated by means of linear regression analysis, to estimate the sign and the average rate of the trend. In addition, the Mann–Kendall test (Kendall, 1975; Mann, 1945) is performed on the time series of the ensemble mean of pr_{Year} and pr_{MAX} , to evaluate the statistical significance of the monotonic trend, independently of its linear or non-linear behaviour.

3.2 Hydrological simulations

Meteorological variables of the seven climate scenarios are regridded at 5 km × 5 km on the simulation domain shown in Fig. 1. For each time step, potential evapotranspiration maps are computed with the module Lisvap (Burek et al., 2013a), using the Penman–Monteith formulation with minimum temperature, maximum temperature, incoming solar radiation, actual vapour pressure and wind speed as input. Actual vapour pressure maps were previously calculated from surface air pressure and specific humidity using the ideal gas formula. The hydrological model Lisflood is then run for the period 1970–2005 and for the future climate scenarios 2006–2100 forced by RCP8.5, using daily precipitation, average temperature and potential evapotranspiration maps generated by Lisvap. A Gumbel extreme value distribution fitting is performed on 30 raster maps of annual maximum discharge of the baseline window (1976–2005), using the L-moments approach (Hosking, 1990). The analytical functions thus derived are used to estimate extreme discharge peaks with chosen return period $Q(RP)$, by inverting the formulation of the Gumbel distribution:

$$Q(RP) = \xi - \alpha \ln \left(-\ln \left(1 - \frac{1}{RP} \right) \right), \quad (2)$$

where α and ξ are the scale and location parameters of the analytical Gumbel distributions.

The peak discharge corresponding to the 2-year return period is commonly considered representative of river bankfull conditions (e.g. Carpenter et al., 1999). Hence, discharge peaks exceeding $Q(RP = 2)$ and their corresponding time of occurrence were extracted from the hydrological simulations of baseline and climate scenarios using the peak over threshold (POT) approach described in Sect. 3.4.

3.3 Quantitative streamflow analysis

The quantitative analysis of simulated streamflow is performed in a similar way as that for precipitation, by comparing the three future time slices against the baseline. The analysis focuses on three variables: the average streamflow \bar{Q} , the mean annual daily peak flow \bar{Q}_{MAX} and the 100-year daily peak flow Q_{100} . Both \bar{Q} and \bar{Q}_{MAX} are extracted directly from the model output, and are robust estimators used as benchmark values for water resources management and peak discharge analysis, respectively. The Q_{100} is instead estimated from the analytical extreme value distribution fitted on the series of annual maxima and is therefore affected by an additional error component. However it is commonly used in flood hazard estimation (Alfieri et al., 2014b; Di Baldassarre et al., 2010; Hall et al., 2005; Merz et al., 2008) as it is a standard in the design of flood protections and often a potential threat to population and assets in case of failure of flood defences.

3.4 Flood frequency analysis

The final set of analyses is specifically addressed at detecting changes in the frequency of extreme peak discharges in each of the three future time slices, as compared to the baseline. The first of these analyses is focused on peak flows with return periods larger than 2 years and it is performed on each grid point of the European river network, given the robustness of the sample data set. Indeed, by definition these events occur with an average frequency of $f_2 = 0.5$ events per year, which lead to a theoretical sample size of 15 events per ensemble member (i.e. 30 years × 0.5 = 15 events) for each grid point.

The second analysis investigates changes in the frequency of extreme events with return periods equal or larger than 100 years, in the three time slices. One can note that such events occur with a theoretical frequency of 0.01 per year and therefore 0.3 times every 30 years. To increase the robustness of the samples, results are aggregated at river basin and country levels. Two-proportion z test is applied to test the statistical significance of expected changes in the frequency of extreme events.

The frequency analysis of extreme events is based on a POT approach on the discharge time series of historical and future scenarios. A new algorithm was developed to select peak discharges from each grid point of the river network of a map stack of daily discharge over Europe. The main challenges faced in this task are related to the variable number of flow peaks above the threshold for each grid point and to the different peak timing. On the other hand the recursive application of the standard POT selection on each grid point is not a viable solution due to the excessive computation time required (i.e. for comparison, this option would have involved looping over more than 10 billion iterations). The considered threshold value is the 2-year return period Q_2 , taken from

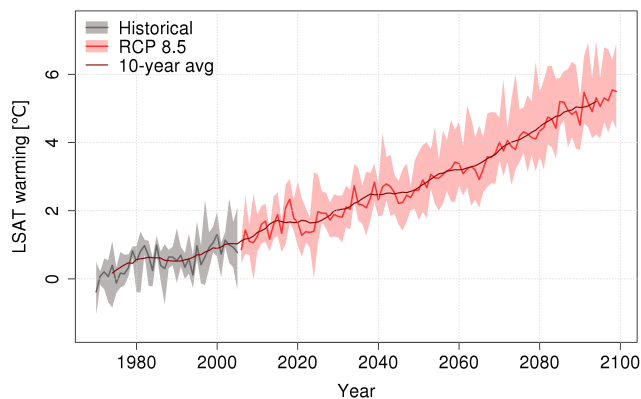


Figure 3. Land surface air temperature warming of the ensemble of seven EURO-CORDEX climate projections compared to pre-industrial times.

the analytical distribution fitted on the historical run of each of the seven climatic scenarios. Each event is defined by the portion of hydrograph larger than Q_2 and it is identified by its peak discharge and the corresponding timing. The selection algorithm was then applied on both the baseline scenarios and the three future time slices, for a total of 43 200–43 830 discharge maps for each model run, depending on the calendar (see Table 1).

4 Results

The ensemble range of the land surface air temperature (LSAT) warming of the seven RCP8.5 scenarios over Europe through the current century is shown in Fig. 3. The warming refers to pre-industrial conditions for consistency with IPCC studies and is obtained by adding a constant value of 0.5°C to the baseline scenario as suggested by Betts et al. (2011) and in agreement with the values reported by the 5th IPCC Assessment Report (IPCC, 2013, Chapter 2). All seven projections exceed the 4°C warming in Europe before the end of the century, with average crossing of the $+2$ and $+4^\circ\text{C}$ occurring in years 2030 and 2073, respectively, based on a 10-year moving average.

4.1 Changes in precipitation

In Fig. 4 (top), the mean annual precipitation (pr_{Year}) and mean annual maximum daily precipitation (pr_{MAX}) are shown for the baseline period, together with the mean relative change (bottom) for the time slice 2080 (i.e. 2066–2095). The ensemble of climate projections agrees on up to a 30% reduction of pr_{Year} in southern European countries, particularly in the Iberian Peninsula, Greece and southern Italy. Conversely, an increasing trend is projected over north-eastern Europe, with the largest changes in Iceland and Scandinavia, while in most of central Europe the ensemble spread is large in comparison to the mean change, so that a

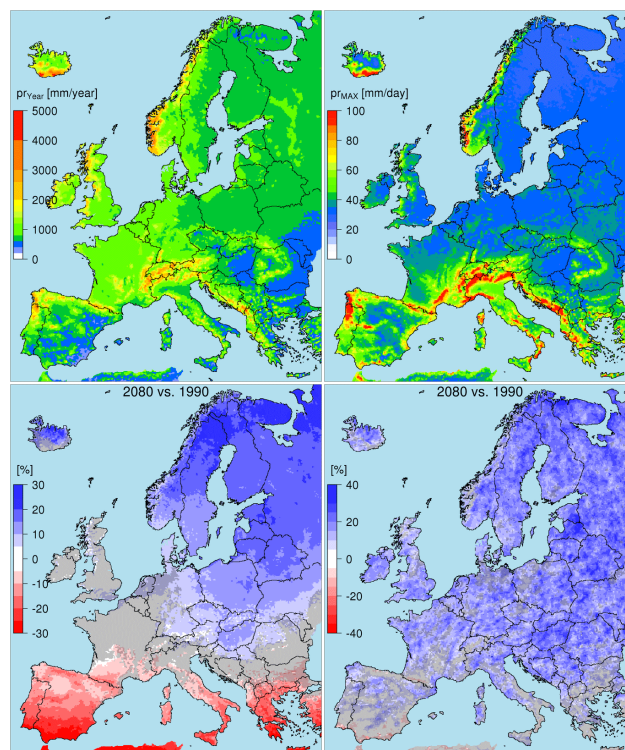


Figure 4. Annual precipitation (pr_{Year} , left) and annual maximum daily precipitation (pr_{MAX} , right). Ensemble mean of the baseline (top) and relative change for the time slice 2066–2095 (bottom). Data points with $CV > 1$ are greyed out.

clear trend cannot be detected (i.e. grey area in Fig. 4 having $CV > 1$). These results are in line with those of the corresponding global climate models of CMIP5 (see Feng et al., 2014; Knutti and Sedláček, 2013), though the regional models give a more detailed representation of the spatial pattern of the projected changes. Significant changes in the future pr_{MAX} are instead mostly positive and have a patchy spatial pattern with the largest values of up to 40% in northern and western Europe (see Fig. 4, bottom-right panel). Changes of pr_{Year} and pr_{MAX} in 2020 and 2050 are shown in Fig. S1 in the Supplement and look like the intermediate conditions between the baseline and 2080, though with a larger proportion of uncertain trends with $CV > 1$.

Annual values of pr_{Year} and pr_{MAX} are analysed at the basin scale for 22 large European river basins. The aims of this analysis are (1) to study long-term trends and the inter-annual variability of the underlying data, (2) to increase the sample robustness through spatial aggregation and detect possible weak but statistically significant trends, and (3) to link basin-wide changes of the precipitation regimes to possible implications on the future runoff. The ensemble range of pr_{Year} and pr_{MAX} for the historical runs and the future scenarios are shown in Fig. 5 for five European river basins shown in green in Fig. 1, together with the ensemble mean and the 10-year moving average (solid lines). In each panel, shades

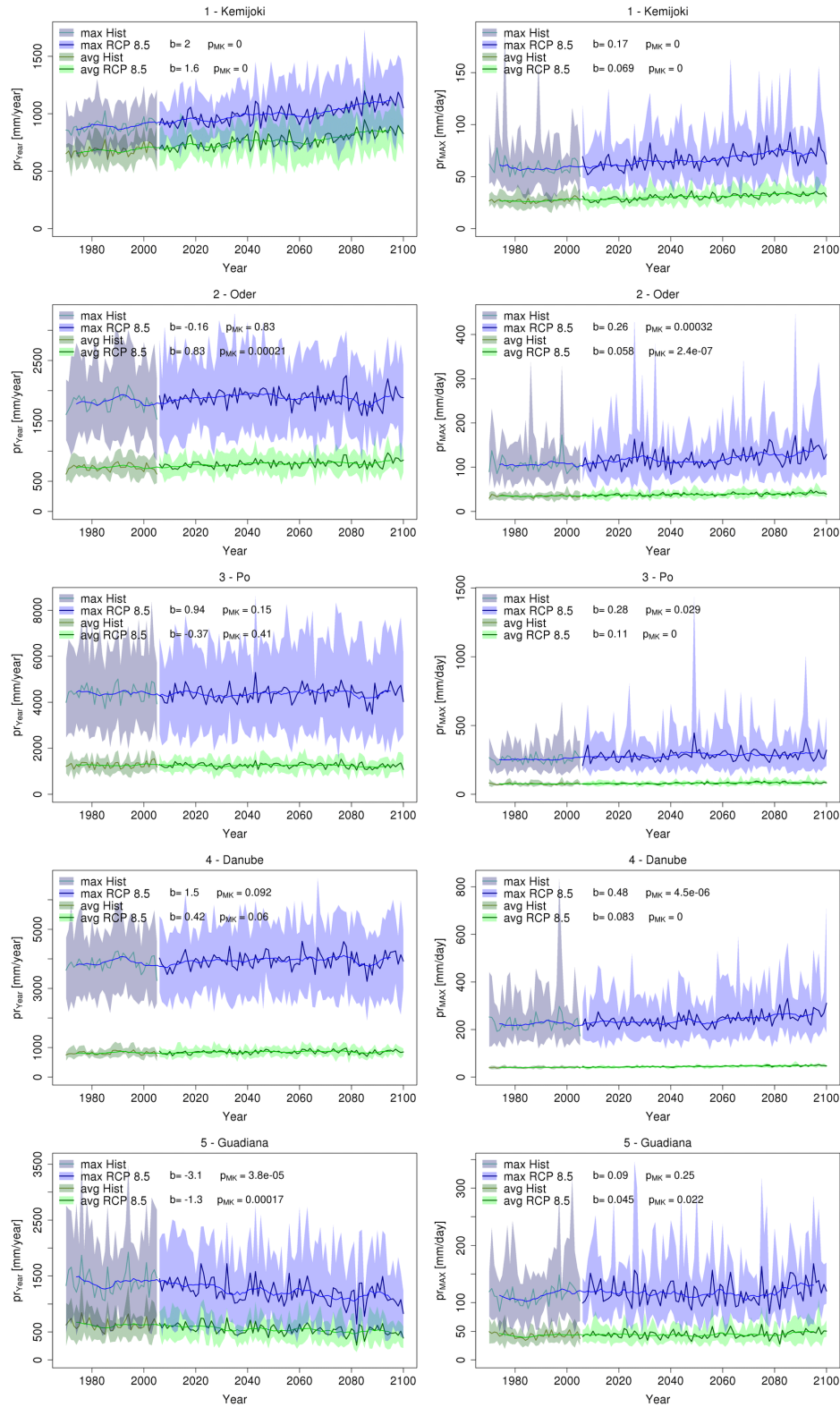


Figure 5. Annual precipitation (pr_{year} , left) and annual maximum daily precipitation (pr_{max} , right) for five European river basins over time. Basin locations are shown in Fig. 1. Basin’s average (green shades) and maximum point value (blue shades) of the ensemble are shown together with the ensemble mean (thick lines) and the 10-year average (thin lines).

of green refer to basin-wide averages, while shades of blue refer to the largest point values within the river basin for each year, independently of their location.

In the two top panels one can see for the Kemijoki River basin a clear rising trend in the mean annual precipitation, with a basin average rate of $b = 1.6 \text{ mm yr}^{-2}$ and point maximum growing at the rate $b = 2 \text{ mm yr}^{-2}$ (i.e. 152 and 190 mm yr^{-1} increase by 2100 , respectively), both statistically significant at $p_{\text{MK}} \approx 0$ using the Mann–Kendall trend test. Similarly, the maximum daily precipitation in the Kemijoki is projected to rise at a basin average rate of $0.07 \text{ mm day}^{-1} \text{ yr}^{-1}$ and at $0.17 \text{ mm day}^{-1} \text{ yr}^{-1}$ for local maxima. Both trends are statistically significant, though with a larger variability between local extremes and basin-wide averages. It is worth noting in Fig. 5 how maximum point accumulations (in blue shades) give a measure of the model's sharpness and of their ability to represent extreme values way larger than climatological averages, yet compatible with realistic observed past values (see e.g. WMO, 2009, Sect. 5.7). An overview of results for the 22 river basins indicates agreement with the pattern shown in Fig. 4. Considering a statistical significance level of 5% for the Mann–Kendall test, 9 river basins out of 22 will experience a significant rise of p_{Year} , in northern and eastern Europe, while a significant decrease of p_{Year} is foreseen in 7 river basins in southern Europe (see Figs. 5 and S2). These figures become 6 and 8, respectively, if point maxima are considered. Significant changes in the future maximum daily precipitation are instead only positive (see Figs. 5 and S3) and are projected to occur in 19 (basin-wide average) and in 15 out of 22 cases (point maximum). The largest significant basin-wide average changes are projected to occur in the Po for p_{MAX} ($+0.11 \text{ mm day}^{-1} \text{ yr}^{-1}$), while for p_{Year} the maximum positive change is in the Neva and Narva ($+1.7 \text{ mm yr}^{-2}$) and the maximum negative in the Guadalquivir (-1.9 mm yr^{-2}).

4.2 Changes in streamflow

Figure 6 (left column) shows the ensemble mean of the average streamflow \bar{Q} , of the mean annual daily peak flow \bar{Q}_{MAX} , and of the 100-year daily peak flow Q_{100} for the baseline scenario, while the relative changes for the time slice 2080 are shown on the right. The corresponding changes for 2020 and 2050 are shown in Fig. S4. Changes in \bar{Q} reproduce similar patterns as those of the mean annual precipitation in Fig. 4, with negative changes in southern Europe, positive in northern and eastern Europe, and uncertain behaviour in the western part of central Europe where $\text{CV} > 1$ over a large area. In the considered study region, \bar{Q} is projected to increase in 73% of the river network by 2080, while the overall mean relative change is 8%. However, the largest projected changes of \bar{Q} are negative and in some cases lower than -40% in southern Spain. One can note that such changes are in absolute value larger than the corresponding reduction in the annual precipitation ($\sim 30\%$ for the same

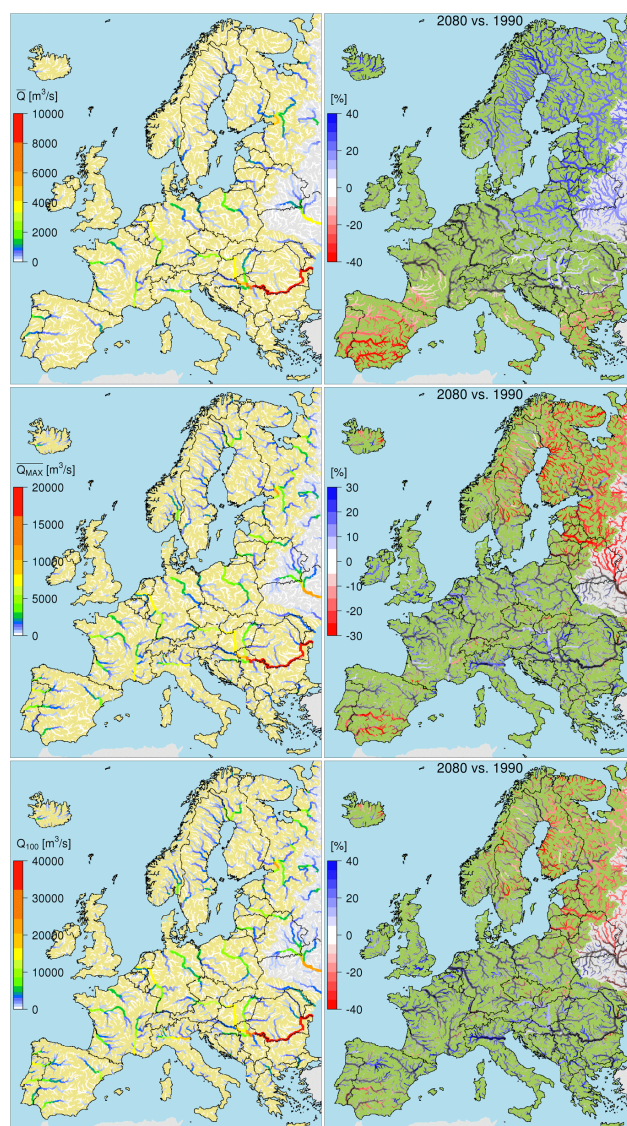


Figure 6. Average streamflow \bar{Q} (top), mean annual daily peak flow \bar{Q}_{MAX} (centre) and 100-year daily peak flow Q_{100} (bottom). Ensemble mean of the baseline (1976–2005) and relative change for the time slice 2066–2095. Data points with $\text{CV} > 1$ are greyed out.

area), as a consequence of the increased evapotranspiration rates caused by the projected warming.

Changes of \bar{Q}_{MAX} and Q_{100} in the three future time slices have similar patterns. Although in the majority of the river network the projected changes have large uncertainty ($\text{CV} > 1$), some significant trends are found, particularly in 2080, where in 38 (for \bar{Q}_{MAX}) and 27% (for Q_{100}) of the river network the ensemble of climate projections points towards a clear change from the baseline. For both variables, positive changes are found in central and southern Europe, though with a rather discontinuous pattern and the alternation of good and poor agreement of the ensemble models. Significant negative changes are instead mainly located in

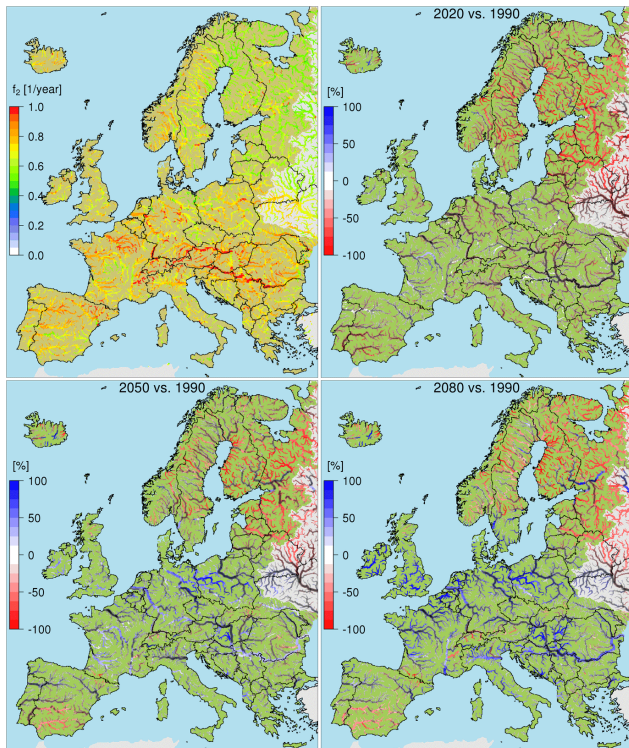


Figure 7. Average frequency of peak flow events with return periods larger than 2 years. Baseline (top left) and relative change for the three future time slices. Data points with $CV > 1$ are greyed out.

southern Spain and in north-eastern Europe, including the Baltic countries, Scandinavia and north-western Russia. For the Iberian case, reasons are sought in the overall reduction in the components contributing to the surface runoff of rivers. On the other hand, negative changes in northern Europe are likely to be linked to the temperature rise and the consequent reduced contribution of snow accumulation and melting on spring floods, as already found in previous studies (Dankers and Feyen, 2008; Kundzewicz et al., 2006).

4.3 Frequency of extreme events

The average annual frequency of peak discharges larger than Q_2 , for brevity referred to as f_2 , is shown in Fig. 7 for the baseline scenario (top left), together with the relative changes for the three future time slices. It is not surprising to see several river reaches with f_2 considerably larger than the theoretical frequency of 0.5. Indeed the analytical distributions are fitted on the samples of annual maxima (i.e. one event per year), while the empirical frequencies in Fig. 7 are counted on the entire time series. As shown by Mallakpour and Villarini (2015), this approach enables a more consistent assessment of event frequency, particularly for those years when more than one event above threshold is recorded. In the future scenarios, changes are particularly consistent in the north-eastern Europe, where a reduction of the frequency

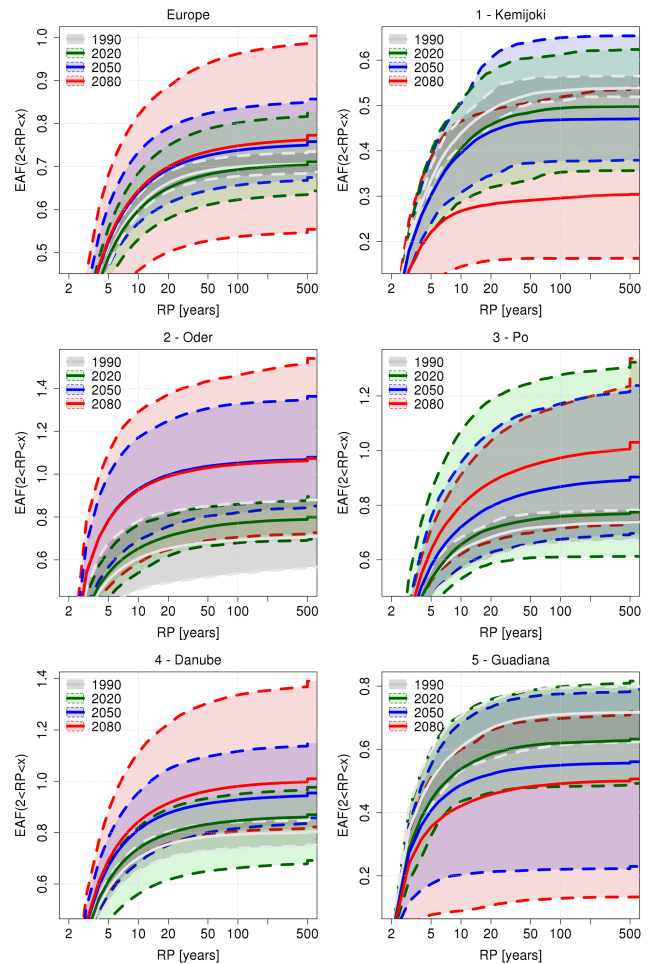


Figure 8. Expected annual frequency of peak flows with return periods larger than 2 years for selected European river basins (see location in Fig. 1) for the baseline simulation and the three future time slices.

of extreme events is clearly visible since the first time slice. In 2080, the pattern of projected relative changes looks similar to that of \bar{Q}_{MAX} in Fig. 6, though with a wider range, where 50 % of grid points exhibit changes in absolute value larger than 35 %.

The expected annual frequency (EAF) of peak flow events larger than Q_2 is shown in Figs. 8 and S5, by aggregating output for the 22 large European river basins considered in this study. Figure 8 also includes Europe-wide aggregated data (top-left panel). For each time slice, the ensemble mean and range are shown with a solid line and a colour shading delimited by dashed lines. The information content of this graphical representation is manifold, and the main points are summarized in the following:

- The y axis shows the EAF of peak flow events with return periods between 2 and any chosen value of the abscissa up to 500 years. Return periods are calculated by inverting Eq. (2), using the discharge peaks over thresh-

Table 2. Mean annual exceedance frequency of the 100-year return period peak flow for different European countries and percentage change between the baseline and the future time slices. Changes in bold are not significant at 1 %.

Country code	Ne	f_{100}				Δf_{100}		
		1990	2020	2050	2080	2020	2050	2080
AL	299	0.0096	0.0123	0.0405	0.0322	29 %	324 %	237 %
AT	672	0.0067	0.0170	0.0253	0.0311	152 %	276 %	362 %
BA	611	0.0096	0.0148	0.0278	0.0309	55 %	191 %	223 %
BE	355	0.0102	0.0336	0.0300	0.0454	228 %	193 %	343 %
BG	1871	0.0159	0.0241	0.0307	0.0319	52 %	94 %	101 %
BY	2098	0.0083	0.0127	0.0143	0.0153	53 %	72 %	84 %
CH	173	0.0036	0.0122	0.0128	0.0223	238 %	254 %	518 %
CZ	1228	0.0140	0.0234	0.0211	0.0244	67 %	50 %	74 %
DE	4750	0.0115	0.0241	0.0219	0.0274	110 %	91 %	139 %
DK	195	0.0179	0.0238	0.0125	0.0329	33 %	-30 %	84 %
EE	87	0.0025	0.0088	0.0047	0.0116	256 %	92 %	372 %
ES	4679	0.0090	0.0164	0.0206	0.0259	83 %	130 %	188 %
FI	1190	0.0031	0.0036	0.0030	0.0036	18 %	-3 %	18 %
FR	6154	0.0094	0.0213	0.0238	0.0324	127 %	154 %	245 %
GR	863	0.0113	0.0269	0.0263	0.0373	137 %	132 %	230 %
HR	353	0.0062	0.0133	0.0255	0.0237	114 %	310 %	280 %
HU	1043	0.0087	0.0194	0.0225	0.0213	122 %	158 %	143 %
IE	442	0.0086	0.0168	0.0196	0.0400	97 %	129 %	368 %
IS	148	0.0020	0.0060	0.0162	0.0221	193 %	695 %	982 %
IT	3734	0.0126	0.0186	0.0340	0.0474	48 %	170 %	276 %
KS	81	0.0088	0.0297	0.0537	0.0444	238 %	512 %	406 %
LT	527	0.0078	0.0148	0.0159	0.0114	89 %	103 %	46 %
LU	17	0.0058	0.0139	0.0173	0.0224	141 %	200 %	288 %
LV	367	0.0054	0.0122	0.0158	0.0185	125 %	192 %	242 %
MD	772	0.0203	0.0370	0.0359	0.0316	82 %	77 %	56 %
ME	118	0.0089	0.0202	0.0320	0.0432	126 %	258 %	384 %
MK	334	0.0120	0.0175	0.0417	0.0403	45 %	246 %	234 %
NL	380	0.0090	0.0340	0.0300	0.0514	276 %	232 %	468 %
NO	627	0.0027	0.0073	0.0086	0.0084	166 %	213 %	207 %
PL	4384	0.0125	0.0283	0.0233	0.0242	127 %	86 %	94 %
PT	684	0.0074	0.0143	0.0184	0.0161	93 %	148 %	118 %
RO	2585	0.0088	0.0222	0.0224	0.0286	151 %	153 %	225 %
RS	883	0.0091	0.0204	0.0345	0.0338	125 %	281 %	273 %
SE	1507	0.0029	0.0064	0.0061	0.0081	123 %	113 %	184 %
SI	135	0.0061	0.0185	0.0316	0.0316	204 %	421 %	421 %
SK	310	0.0050	0.0165	0.0126	0.0134	232 %	153 %	169 %
UK	2012	0.0120	0.0191	0.0240	0.0403	59 %	101 %	237 %
Europe	51 154	0.0080	0.0159	0.0181	0.0222	97 %	126 %	176 %

old extracted from the hydrological simulations. Peak flows above a 500-year return period are added as lump contribution at the position $x = 500$ years of the abscissa. In other words, values at the far right of the abscissa are read as $EAF(2 < RP < \infty) \equiv f_2$, as those in Fig. 8. It is worth noting that the estimated return period of simulated flood peaks of both the baseline and the future time slices is derived from the corresponding analytical extreme value distribution computed only on the baseline scenario. This step is crucial to compute coherent estimates of future extremes with return periods

larger than the length of the time slice and thus represent a substantial improvement as compared to approaches comparing statistical values with the same probability of occurrence but taken from different analytical distributions.

- In each graph one can follow the expected mean change in the frequency of extreme events through the three time slices (solid lines), while the ensemble spread gives a measure of the uncertainty in the climate projections. In most river basins, the ensemble uncertainty is wider in the last time slice (i.e. 2080, in pink shades), though

for some cases this occurs in the 2050 (i.e. Duero, Ebro, Maritsa, Tagus) and even in the 2020 time slice (i.e. Po, Garonne, Loire).

- Graphs in Fig. 8 give an insight into the distribution of events with different return periods. Indeed, the first derivative of the mean EAF (i.e. the local slope) indicates the expected frequency of events for any selected return period. In addition, one can estimate the EAF of events above any chosen threshold T_1 , with the equation

$$\text{EAF}(\text{RP} \geq T_1) \equiv f_{T_1} = f_2 - \text{EAF}(\text{RP} < T_1), \quad (3)$$

where both terms of the difference can be read on the graph. For example, in Europe (Fig. 8, top-left panel), the frequency of events above 2 years in the baseline (i.e. 1990) is $f_2 = 0.709 \text{ events yr}^{-1}$, while the expected frequency of events below 100 years is $\text{EAF}(\text{RP} < 100) = 0.701$, leading to an average frequency $\text{EAF}(\text{RP} \geq 100) \equiv f_{100} \approx 0.8\%$, rather similar to the theoretical frequency of 1%. If one considers for the same region the time slice 2020, the frequency $f_2 = 0.711 \text{ events yr}^{-1}$ is very similar to that of the baseline. However, the frequency $\text{EAF}(\text{RP} < 100) = 0.695$ is considerably lower, leading to an expected annual frequency $f_{100} \approx 1.6\%$ and a consequent increase by 97% of peak flows with return periods above 100 years. Conversely, it is interesting to note that the frequency of low return period events (e.g. 20 years) is projected to decrease in time slice 2020 as compared to the baseline. Similarly, in the time slices 2050 and 2080, f_{100} is projected to increase by 126 and 176% (see Table 2), though with substantial increase of the frequency of events with lower magnitude too.

The frequency analysis of extreme peak flow events above a 100-year return period is of particular interest, given that the average protection level of the European river network is of the same magnitude (Rojas et al., 2013), with some obvious differences among different countries and river basins (Jongman et al., 2014). In other words, a substantial increase in the frequency of peak flows below the protection level is likely to have a lower impact, in terms of population affected and economic losses, in comparison to a small but significant change in extreme events causing settled areas to be inundated by the flood flow. In this regard, Figs. 8 and S5 denote a visible increase of extreme events above a 500-year return period in a number of river basins (e.g. Po, Dniester, Duero, Garonne, Ebro, Loire, Maritsa, Rhine, Rhone), including some where the overall frequency f_2 of events above threshold is projected to decrease (e.g. Guadiana, Narva). A summary of country-aggregated estimates of f_{100} and the relative changes from the baseline in future time slices is shown in Table 2. Values are obtained by counting the average frequency of occurrence in all grid points of the river network

within each country. It is worth noting that larger countries have on average a larger sample of historical events (N_e) with return periods larger than 100 years to estimate relative changes. The statistical significance of the estimated change in the ensemble mean was tested with a two-proportion z test. A stringent p value of 1‰ is chosen as threshold for significance, to compensate for the autocorrelation of extreme events in neighbouring grid points along the drainage direction. In addition, this issue is mitigated by the use of an ensemble of seven independent models.

The striking outcome of Table 2 is the large dominance of positive changes in f_{100} since the first future time slice, although in some areas the overall frequency f_2 of peak flows over threshold is projected to decrease considerably, such as in Spain (Guadiana and Guadalquivir) and in some river basins in north-eastern Europe (Kemijoki, Daugava, Neva and Narva) as shown in Figs. 8 and S5. In time slice 2080, projected changes are positive and significant in all the considered countries, with values ranging between 18% in Finland and up to 982% in Iceland.

5 Discussion

The outcomes of the analyses carried out show some similarities with previous literature works. Using global climate scenarios from the CMIP5 data set based on RCP, Dankers et al. (2013) and Hirabayashi et al. (2013) noted a reduction of the magnitude of extreme discharge peaks in eastern Europe by year 2100, while some increase was found over western Europe. However, local patterns of variability are not detected by global models using input data and impact models at relatively coarse resolution, particularly due to the averaging effect induced by smoothed weather extremes and simplified river network. On the other hand, mean annual precipitation and average discharges estimated in this study have similar pattern to those found by Dankers and Feyen (2008) and by Rojas et al. (2012) in the context of regional studies over Europe. The first work is based on RCM scenarios from the HIRHAM model with 12 km horizontal resolution, belonging to the PRUDENCE data set. The latter is instead based on bias-corrected SRES scenarios at 25 km resolution, coming from the ENSEMBLES project. Interestingly, projections of Q_{100} by Dankers and Feyen (2008) show several common features with the findings of this study, with consistent decrease in Finland, Baltic countries and southern Spain, and the central part of Europe showing widespread increase of Q_{100} , though with larger model variability and local disagreement on the sign of the change. In the work of Rojas et al. (2012), some common features with this work are preserved, though in the former, the region subject to a decrease in Q_{100} looks shifted southward towards Poland, Slovakia and part of Bulgaria. Both previous studies were focused on the change of extreme discharges by comparing analytical distributions fitted on different samples of annual maxima.

Such approach brings three main limitations: (1) it favours the change in magnitude rather than in frequency of events, given that only the largest annual discharge peak is considered even when more than one extreme event occurs; (2) it relies on the estimation of events with theoretical frequency of occurrence (1 in 100 years) below that used to fit the analytical distributions (i.e. 1 in 30 years), leading to increased uncertainty range; and (3) it includes the uncertainty contribution of two analytical distributions, that is, one for the sample of historical peaks and one for the future peaks. The methodology proposed in this work addresses two of the three issues by selecting the simulated peaks above a critical threshold, both for the baseline and the future time slices. The expected frequency (and in turn the return period) of these peaks is evaluated through the use of only one analytical distribution, i.e. that of the historical run. Hence, the comparison of the return period of past and future events is more consistent, so that the remaining uncertainty is only on the estimated frequency of occurrence (i.e. point 2 described above). This limitation is difficult to address as the aim of our work is to detect climatic changes within the time range of a century, over which the hypothesis of stationarity of the extremes cannot be laid. Furthermore, as only one analytical distribution is used to convert discharge peaks into return periods, the ranking among historical and future events is preserved. In other words, the uncertainty of the extreme value distribution fitting has a limited impact on the outcomes of the frequency analysis, since the key message can also be formulated as “widespread increase in frequency of extreme floods, independently from the changes in frequency of events with lower magnitude.”

Some further words should address the use of the CV to evaluate the agreement of projected changes. The CV accounts for both the spread and the mean value of a distribution; hence, it gives a better assessment of the consistency of a sample distribution compared to methods focused on the agreement of the sign of the change (e.g. Koirala et al., 2014; Rojas et al., 2012; Tebaldi et al., 2011). The CV gives a measure of the signal-to-noise ratio and it has strong similarities to the robustness measure described by Knutti and Sedláček (2013). However, the latter compares an ensemble of projections against one reference historical run. On the other hand, the proposed approach is particularly suitable for climate scenarios, where each future projection is compared to the corresponding baseline run, representative of the historical conditions. In this way, the model consistency is maximized so that the model agreement is assessed on the ensemble of relative changes, rather than of absolute values. The presented methodology draws on some concepts commonly used in the field of ensemble flood early warning, where the use of model consistent climatologies can provide a calibration effect and was shown to be a key step to skillfully detect deviations from reference values or the exceedance of statistical thresholds (Alfieri et al., 2014a; Diomede et al., 2014; Fundel et al., 2010).

6 Conclusions

This work investigates the implications of high-end climate scenarios on future hydro-meteorological patterns over Europe, with focus on extreme events potentially dangerous for assets and population. The adopted methodology includes the following novelties.

- Changes in the frequency of future extreme peak flows are evaluated on the sample of simulated peaks over threshold, rather than on values taken from the analytical curves fitted on the sample of selected maxima. This enables a more consistent evaluation (1) of the frequency of extreme events and (2) of relative changes between the baseline and the future scenarios, thanks to the use of the same frequency distribution (i.e. of the baseline) as reference for the comparison.
- An improved evaluation and visualization of the uncertainty is hereby proposed, based on the coefficient of variation computed on the ensemble of relative changes of the model projections. The proposed method is similar to that used in previous studies, though it is more suitable to detect variations of an ensemble of projections, each with a relative baseline simulation.

Results of this work indicate strong model agreement in the projected change of average inflow and runoff in the European river network. By the end of the century, both mean annual precipitation and average discharge are projected to decrease in southern Europe and to increase in north-eastern Europe, while in central Europe the ensemble of projections does not agree on a specific trend. Projected changes in extreme values are on average less significant and show different spatial patterns for precipitation and discharge. On the one hand, a positive trend for the maximum daily precipitation is found in most of the study region, with both magnitude and statistical significance becoming stronger moving towards eastern and northern Europe. On the other hand, the trend of future discharge extremes has a rather different pattern, as a consequence of the interplay among various hydrological processes, which includes the effects of a warming climate on the reduced snow accumulation cycle and the growth of evapotranspiration rates. As a result, we found a reduction of peak discharges in southern Spain, Scandinavia and Baltic countries, while a large portion of central Europe including the British Isles are likely to experience a progressive increase in the magnitude and frequency of discharge peaks.

Finally, a frequency analysis on simulated peaks over a threshold revealed further insight on the distribution of future extreme peak flows in Europe. Interestingly, the expected annual frequency of events with peak discharge above the 100-year return period is projected to rise significantly in most of the considered European countries, including some where the overall number of severe events (i.e. larger than Q_2) is

likely to decrease. The projected figures are unsettling, showing significant increase in the frequency of extreme events larger than 100 % in 21 out of 37 European countries since the first time slice (2006–2035), and a further deterioration in the subsequent future. These findings relate to a range of event magnitude mostly above the average protection level of European rivers, hence they have serious implications on the associated flood risk and the potential impact on business and society.

The Supplement related to this article is available online at doi:10.5194/hess-19-2247-2015-supplement.

Acknowledgements. The research leading to these results has received funding from the European Union Seventh Framework Programme FP7/2007-2013 under grant agreement no. 603864 (HELIX: High-End cLimate Impacts and eXtremes; <http://www.helixclimate.eu>).

Edited by: M. Werner

References

- Alfieri, L., Thielen, J., and Pappenberger, F.: Ensemble hydro-meteorological simulation for flash flood early detection in southern Switzerland, *J. Hydrol.*, 424–425, 143–153, doi:10.1016/j.jhydrol.2011.12.038, 2012.
- Alfieri, L., Pappenberger, F., and Wetterhall, F.: The extreme runoff index for flood early warning in Europe, *Nat. Hazards Earth Syst. Sci.*, 14, 1505–1515, doi:10.5194/nhess-14-1505-2014, 2014a.
- Alfieri, L., Salamon, P., Bianchi, A., Neal, J., Bates, P., and Feyen, L.: Advances in pan-European flood hazard mapping, *Hydrol. Process.*, 28, 4067–4077, doi:10.1002/hyp.9947, 2014b.
- Alkama, R., Marchand, L., Ribes, A., and Decharme, B.: Detection of global runoff changes: Results from observations and CMIP5 experiments, *Hydrol. Earth Syst. Sci.*, 17, 2967–2979, doi:10.5194/hess-17-2967-2013, 2013.
- Andersen, T. K. and Marshall Shepherd, J.: Floods in a changing climate, *Geogr. Compass*, 7, 95–115, doi:10.1111/gec3.12025, 2013.
- Arnell, N. W. and Gosling, S. N.: The impacts of climate change on river flood risk at the global scale, *Climatic Change*, 1–15, doi:10.1007/s10584-014-1084-5, 2014.
- Betts, R. A., Collins, M., Hemming, D. L., Jones, C. D., Lowe, J. A., and Sanderson, M. G.: When could global warming reach 4 °C?, *Philos. T. Roy. Soc. A*, 369, 67–84, 2011.
- Burek, P., van der Knijff, J., and Ntegeka, V.: LISVAP, Evaporation Pre-Processor for the LISFLOOD Water Balance and Flood Simulation Model – Revised User Manual, EUR 26167 EN, Joint Research Centre – Institute for Environment and Sustainability, doi:10.2788/2498, 36 pp., 2013a.
- Burek, P., Knijff van der, J., and Roo de, A.: LISFLOOD, distributed water balance and flood simulation model revised user manual 2013, Publications Office, Luxembourg, available at: <http://dx.publications.europa.eu/10.2788/24719> (last access: 12 December 2014), 2013b.
- Carpenter, T. M., Sperfslage, J. A., Georgakakos, K. P., Sweeney, T., and Fread, D. L.: National threshold runoff estimation utilizing GIS in support of operational flash flood warning systems, *J. Hydrol.*, 224, 21–44, 1999.
- Christensen, J. H., Carter, T. R., Rummukainen, M., and Amanatidis, G.: Evaluating the performance and utility of regional climate models: The PRUDENCE project, *Climatic Change*, 81, 1–6, doi:10.1007/s10584-006-9211-6, 2007.
- Dankers, R. and Feyen, L.: Climate change impact on flood hazard in Europe: An assessment based on high-resolution climate simulations, *J. Geophys. Res.-Atmos.*, 113, D19105, doi:10.1029/2007JD009719, 2008.
- Dankers, R. and Feyen, L.: Flood hazard in Europe in an ensemble of regional climate scenarios, *J. Geophys. Res.-Atmos.*, 114, D16108, doi:10.1029/2008JD011523, 2009.
- Dankers, R., Arnell, N. W., Clark, D. B., Falloon, P. D., Fekete, B. M., Gosling, S. N., Heinke, J., Kim, H., Masaki, Y., Satoh, Y., Stacke, T., Wada, Y., and Wisser, D.: First look at changes in flood hazard in the Inter-Sectoral Impact Model Intercomparison Project ensemble, *P. Natl. Acad. Sci. USA*, 111, 3257–3261, doi:10.1073/pnas.1302078110, 2013.
- De Roo, A., Odiijk, M., Schmuck, G., Koster, E., and Lucieer, A.: Assessing the effects of land use changes on floods in the meuse and oder catchment, *Phys. Chem. Earth B*, 26, 593–599, 2001.
- Di Baldassarre, G., Schumann, G., Bates, P. D., Freer, J. E., and Beven, K. J.: Flood-plain mapping: A critical discussion of deterministic and probabilistic approaches, *Hydrolog. Sci. J.*, 55, 364–376, doi:10.1080/02626661003683389, 2010.
- Diomede, T., Marsigli, C., Montani, A., Nerozzi, F., and Paccagnella, T.: Calibration of Limited-Area Ensemble Precipitation Forecasts for Hydrological Predictions, *Mon. Weather Rev.*, 142, 2176–2197, doi:10.1175/MWR-D-13-00071.1, 2014.
- Ehret, U., Zehe, E., Wulfmeyer, V., Warrach-Sagi, K., and Liebert, J.: HESS Opinions “Should we apply bias correction to global and regional climate model data?”, *Hydrol. Earth Syst. Sci.*, 16, 3391–3404, doi:10.5194/hess-16-3391-2012, 2012.
- Feng, S., Hu, Q., Huang, W., Ho, C.-H., Li, R., and Tang, Z.: Projected climate regime shift under future global warming from multi-model, multi-scenario CMIP5 simulations, *Global Planet. Change*, 112, 41–52, doi:10.1016/j.gloplacha.2013.11.002, 2014.
- Field, C. B., Barros, V. R., Mach, K. J., Mastrandrea, M. D., van Aalst, M., Adger, W. N., Arent, D. J., Barnett, J., Betts, R., Bilir, T. E., Birkmann, J., Carmin, J., Chadee, D. D., Challinor, A. J., Chatterjee, M., Cramer, W., Davidson, D. J., Estrada, Y. O., Gattuso, J.-P., Hijioka, Y., Hoegh-Guldberg, O., Huang, H. Q., Insarov, G. E., Jones, R. N., Kovats, R. S., Romero-Lankao, P., Larsen, J. N., Losada, I. J., Marengo, J. A., McLean, R. F., Mearns, L. O., Mechler, R., Morton, J. F., Niang, I., Oki, T., Olwoch, J. M., Opondo, M., Poloczanska, E. S., Pörtner, H.-O., Redsteer, M. H., Reisinger, A., Revi, A., Schmidt, D. N., Shaw, M. R., Solecki, W., Stone, D. A., Stone, J. M. R., Strzepek, K. M., Suarez, A. G., Tschakert, P., Valentini, R., Viciuña, S., Villamizar, A., Vincent, K. E., Warren, R., White, L. L., Wilbanks, T. J., Wong, P. P., and Yohe, G. W.: Technical summary, in: *Climate Change 2014: Impacts, Adaptation, and Vulnerability, Part A: Global and Sectoral Aspects, Contribution of Working Group II to the Fifth Assessment Report of the Intergovernmental Panel on Climate Change*, edited by: Field, C. B., Barros, V.

- R., Dokken, D. J., Mach, K. J., Mastrandrea, M. D., Bilir, T. E., Chatterjee, M., Ebi, K. L., Estrada, Y. O., Genova, R. C., Girma, B., Kissel, E. S., Levy, A. N., MacCracken, S., Mastrandrea, P. R., and White, L. L., Cambridge University Press, Cambridge, UK and New York, NY, USA, 35–94, 2014.
- Fundel, F., Walser, A., Liniger, M. A., and Appenzeller, C.: Calibrated precipitation forecasts for a limited-area ensemble forecast system using reforecasts, *Mon. Weather Rev.*, 138, 176–189, 2010.
- Hall, J. W., Sayers, P. B., and Dawson, R. J.: National-scale assessment of current and future flood risk in England and Wales, *Nat. Hazards*, 36, 147–164, 2005.
- Hirabayashi, Y., Mahendran, R., Koirala, S., Konoshima, L., Yamazaki, D., Watanabe, S., Kim, H., and Kanae, S.: Global flood risk under climate change, *Nat. Clim. Change*, 3, 816–821, doi:10.1038/nclimate1911, 2013.
- Hosking, J. R. M.: L-Moments: Analysis and Estimation of Distributions Using Linear Combinations of Order Statistics, *J. R. Stat. Soc. Ser. B*, 52, 105–124, 1990.
- Huang, S., Krysanova, V., and Hattermann, F. F.: Does bias correction increase reliability of flood projections under climate change? A case study of large rivers in Germany, *Int. J. Climatol.*, 34, 3780–3800, doi:10.1002/joc.3945, 2014.
- IPCC: Summary for Policymakers, in: *Climate Change 2007: The Physical Science Basis, Contribution of Working Group I to the Fourth Assessment Report of the Intergovernmental Panel on Climate Change*, edited by: Solomon, S., Qin, D., Manning, D. M., Chen, Z., Marquis, M., Averyt, K. B., Tignor, M., and Miller, H. L., Cambridge University Press, Cambridge, UK and New York, NY, USA, 2007.
- IPCC: Summary for Policymakers, in: *Climate Change 2013: The Physical Science Basis, Contribution of Working Group I to the Fifth Assessment Report of the Intergovernmental Panel on Climate Change*, edited by: Stocker, T. F., Qin, D., Plattner, G.-K., Tignor, M., Allen, S. K., Boschung, J., Nauels, A., Xia, Y., Bex, V., and Midgley, P. M., Cambridge University Press, Cambridge, UK and New York, NY, USA, 2013.
- Jacob, D., Petersen, J., Eggert, B., Alias, A., Christensen, O. B., Bouwer, L. M., Braun, A., Colette, A., Déqué, M., Georgievski, G., Georgopoulou, E., Gobiet, A., Menut, L., Nikulin, G., Haensler, A., Hempelmann, N., Jones, C., Keuler, K., Kovats, S., Kröner, N., Kotlarski, S., Kriegsmann, A., Martin, E., Meijgaard, E. van, Moseley, C., Pfeifer, S., Preuschmann, S., Radermacher, C., Radtke, K., Rechid, D., Rounsevell, M., Samuelsson, P., Somot, S., Soussana, J.-F., Teichmann, C., Valentini, R., Vautard, R., Weber, B., and You, P.: EURO-CORDEX: new high-resolution climate change projections for European impact research, *Reg. Environ. Change*, 14, 563–578, doi:10.1007/s10113-013-0499-2, 2014.
- Jongman, B., Hochrainer-Stigler, S., Feyen, L., Aerts, J. C. J. H., Mechler, R., Botzen, W. J. W., Bouwer, L. M., Pflug, G., Rojas, R., and Ward, P. J.: Increasing stress on disaster-risk finance due to large floods, *Nat. Clim. Change*, 4, 264–268, doi:10.1038/nclimate2124, 2014.
- Kamari, J., Alcamo, J., Barlund, I., Duel, H., Farquharson, F. A. K., Florke, M., Fry, M., Houghton-Carr, H. A., Kabat, P., Kaljonen, M., Kok, K., Meijer, K. S., Rekolainen, S., Sendzimir, J., Varjopuro, R., and Villars, N.: Envisioning the future of water in Europe – the SCENES project, *E-WATER*, 1–28, 2008.
- Kendall, M. G.: *Rank Correlation Methods*, 4th Edn., Charles Griffin, London, 1975.
- Knutti, R. and Sedláček, J.: Robustness and uncertainties in the new CMIP5 climate model projections, *Nat. Clim. Change*, 3, 369–373, doi:10.1038/nclimate1716, 2013.
- Koirala, S., Hirabayashi, Y., Mahendran, R., and Kanae, S.: Global assessment of agreement among streamflow projections using CMIP5 model outputs, *Environ. Res. Lett.*, 9, 064017, doi:10.1088/1748-9326/9/6/064017, 2014.
- Kundzewicz, Z. W., Radziejewski, M., and Pinskiwar, I.: Precipitation extremes in the changing climate of Europe, *Clim. Res.*, 31, 51–58, doi:10.3354/cr031051, 2006.
- Mallakpour, I. and Villarini, G.: The changing nature of flooding across the central United States, *Nat. Clim. Change*, 5, 250–254, doi:10.1038/nclimate2516, 2015.
- Mann, H. B.: Non-parametric tests against trend, *Econometrica*, 13, 163–171, 1945.
- McCarthy, J. J.: *Climate change 2001: impacts, adaptation, and vulnerability: contribution of Working Group II to the third assessment report of the Intergovernmental Panel on Climate Change*, Cambridge University Press, available at: <http://books.google.it/books?hl=it&lr=&id=QSoJdCRvRXQC&oi=fnd&pgPP7&dq=third+assessment+report+ipcc&ots=dT1spJd5eV&sig=dhJsDN-iMjM8rHTTny6mckRVk> (last access: 20 November 2014), 2001.
- Merz, R., Blöschl, G., and Humer, G.: National flood discharge mapping in Austria, *Nat. Hazards*, 46, 53–72, doi:10.1007/s11069-007-9181-7, 2008.
- Muerth, M. J., Gauvin St-Denis, B., Ricard, S., Velázquez, J. A., Schmid, J., Minville, M., Caya, D., Chaumont, D., Ludwig, R., and Turcotte, R.: On the need for bias correction in regional climate scenarios to assess climate change impacts on river runoff, *Hydrol. Earth Syst. Sci.*, 17, 1189–1204, doi:10.5194/hess-17-1189-2013, 2013.
- Ntegeka, V., Salamon, P., Gomes, G., Sint, H., Lorini, V., Thielen, J., and Zambrano-Bigiarini, M.: EFAS-Meteo: A European daily high-resolution gridded meteorological data set for 1990–2011, available at: <http://publicationsjrc.europa.eu/ourtownypd.com/repository/handle/11111111/30589> (last access: 3 June 2014), 2013.
- Perez, J., Menendez, M., Mendez, F. J., and Losada, I. J.: Evaluating the performance of CMIP3 and CMIP5 global climate models over the north-east Atlantic region, *Clim. Dynam.*, 43, 2663–2680, doi:10.1007/s00382-014-2078-8, 2014.
- Rojas, R., Feyen, L., Bianchi, A., and Dosio, A.: Assessment of future flood hazard in Europe using a large ensemble of bias-corrected regional climate simulations, *J. Geophys. Res.-Atmos.*, 117, D17109, doi:10.1029/2012JD017461, 2012.
- Rojas, R., Feyen, L., and Watkiss, P.: Climate change and river floods in the European Union: Socio-economic consequences and the costs and benefits of adaptation, *Global Environ. Change*, 23, 1737–1751, doi:10.1016/j.gloenvcha.2013.08.006, 2013.
- Sperna Weiland, F. C., Van Beek, L. P. H., Weerts, A. H., and Bierkens, M. F. P.: Extracting information from an ensemble of GCMs to reliably assess future global runoff change, *J. Hydrol.*, 412–413, 66–75, doi:10.1016/j.jhydrol.2011.03.047, 2012.
- Taylor, K. E., Stouffer, R. J., and Meehl, G. A.: An Overview of CMIP5 and the Experiment Design, *B. Am. Meteorol. Soc.*, 93, 485–498, doi:10.1175/BAMS-D-11-00094.1, 2012.

- Tebaldi, C., Arblaster, J. M., and Knutti, R.: Mapping model agreement on future climate projections, *Geophys. Res. Lett.*, 38, L23701, doi:10.1029/2011GL049863, 2011.
- Themeßl, M. J., Gobiet, A., and Heinrich, G.: Empirical-statistical downscaling and error correction of regional climate models and its impact on the climate change signal, *Climatic Change*, 112, 449–468, doi:10.1007/s10584-011-0224-4, 2012.
- Thielen, J., Bartholmes, J., Ramos, M.-H., and de Roo, A.: The European Flood Alert System – Part 1: Concept and development, *Hydrol. Earth Syst. Sci.*, 13, 125–140, doi:10.5194/hess-13-125-2009, 2009.
- Thiemig, V., Rojas, R., Zambrano-Bigiarini, M., and De Roo, A.: Hydrological evaluation of satellite-based rainfall estimates over the Volta and Baro-Akobo Basin, *J. Hydrol.*, 499, 324–338, doi:10.1016/j.jhydrol.2013.07.012, 2013.
- Thirel, G., Notarnicola, C., Kalas, M., Zebisch, M., Schellenberger, T., Tetzlaff, A., Duguay, M., Mölg, N., Burek, P., and de Roo, A.: Assessing the quality of a real-time Snow Cover Area product for hydrological applications, *Remote Sens. Environ.*, 127, 271–287, doi:10.1016/j.rse.2012.09.006, 2012.
- Van der Knijff, J. M., Younis, J., and de Roo, A. P. J.: LISFLOOD: A GIS-based distributed model for river basin scale water balance and flood simulation, *Int. J. Geogr. Inf. Sci.*, 24, 189–212, 2010.
- Van der Linden, P. and Mitchell, J. F. B. (Eds.): ENSEMBLES: Climate Change and its Impacts: Summary of research and results from the ENSEMBLES project, Met Off. Hadley Cent., Exeter, UK, 1–160, 2009.
- Wanders, N., Bierkens, M. F. P., de Jong, S. M., de Roo, A., and Karssenber, D.: The benefits of using remotely sensed soil moisture in parameter identification of large-scale hydrological models, *Water Resour. Res.*, 50, 6874–6891, doi:10.1002/2013WR014639, 2014.
- WMO: Guide to Hydrological Practices, Vol. 2, 6th Edn., Geneva, Switzerland, 2009.
- Younis, J., Anquetin, S., and Thielen, J.: The benefit of high-resolution operational weather forecasts for flash flood warning, *Hydrol. Earth Syst. Sci.*, 12, 1039–1051, doi:10.5194/hess-12-1039-2008, 2008.
- Zambrano-Bigiarini, M. and Rojas, R.: hydroPSO: Particle Swarm Optimisation, with focus on Environmental Models, available at: <http://cran.r-project.org/web/packages/hydroPSO/index.html>, last access: 28 May 2014.